Available online at www.sciencedirect.com
ScienceDirect
Trans. Nonferrous Met. Soc. China 33(2023) 1331−1344
Transactions of Nonferrous Metals Society of China
www.tnmsc.cn

Coupling analysis on controlling mechanisms for creep of Al−Fe−Ni alloy

Ze-yu BIAN[1,2,3], Ai-lin ZHU[1,2], Ya-kai XIAO[1,2], Yu-gang LI[1],
Nai-heng MA[1,4], Han-bing BIAN[3], Ming-liang WANG[1], Zhe CHEN[2], Hao-wei WANG[1,2]

1. State Key Laboratory of Metal Matrix Composites, Shanghai Jiao Tong University, Shanghai 200240, China;
2. School of Materials Science and Engineering, Shanghai Jiao Tong University, Shanghai 200240, China;
3. Laboratoire de Génie Civil et Géo-Environnement, Université de Lille, F-59000 Lille, France;
4. Anhui Aluminium Matrix Composites Engineering Research Centre, Huaibei 235000, China

Received 16 December 2021; accepted 11 April 2022

Abstract: The dislocation creep of Al−Fe−Ni alloy at both 300 and 400 °C was described by a coupling modification on analyzing the creep constitutive equation after introducing both threshold stress and load transfer coefficient. The quantitative results and microstructure characterizations showed that the complex interaction between dislocation and eutectic phase was the origin of threshold stress, and the modulus difference between matrix and eutectic phase induced the load transfer effect. Furthermore, the temperature effects on the modulus of matrix and eutectic phase were different, leading to the decline of threshold stress and increase of load transfer coefficient at higher temperatures. This was further evidenced by the finite element modelling analysis. Finally, the controlling mechanisms during dislocation creep of eutectic alloys were discussed in an increasingly quantitative manner.

Key words: dislocation creep; aluminum alloy; eutectic phase; load transfer effect; threshold stress

1 Introduction

With the development of industrial fields, the metallic materials are increasingly demanded for the improved high temperature (HT) performance [1−3]. Specifically, the applied alloys are expected to be lighter during 200−400 °C with lower cost. The improvement of heat-resistant Al alloys possesses the best potential to meet these requirements [4,5]. In recent years, there are many attempts to improve heat-resistant Al alloys, which can be divided into following strategies.

(1) The lower diffusion elements (i.e. Sc, Mn and Zr) are micro-alloyed into the traditional heat-resistant Al−Si or Al−Cu alloys. Then, the main strengthening phases (i.e. Si or Al_2Cu) can be stabilized at HTs by interfacial adsorption of micro-alloyed elements. Indeed, several successful examples are reported, including Al−Si−Sc−(Zr) [6], Al−Cu−Sc [7,8], and Al−Cu−Mn−Zr [9] alloys.

(2) The highly stable precipitates or secondary phases from Al matrix can improve the thermal stability of alloys. Generally, the introduction of HT stable precipitates (i.e. Al_3(Sc,Zr), Al_6(Mn,Si)) effectively impedes dislocation movement and prevents deformation in Al−Sc−Zr [10,11] and Al−Mn−Mg−Si [12] alloys. Furthermore, the secondary phase stabilized at HTs can form eutectic frame with the large volume fraction during solidification, sharing the stress applied on the matrix to improve HT performance, i.e. Al−Ni [13], Al−Fe−Ni [14,15], and Al−RE [16] alloys.

(3) The introduction of ceramic particles is an effective method to reinforce Al-based materials. Owing to their higher melting points, both ex-situ

Corresponding author: Ming-liang WANG, Tel: +86-21-34202540, E-mail: mingliang_wang@sjtu.edu.cn;
Zhe CHEN, Tel: +86-21-54747597, E-mail: zhe.chen@sjtu.edu.cn
DOI: 10.1016/S1003-6326(23)66186-2

added and in-situ formed particles can improve the HT performance of Al matrix composite, i.e. Al−TiB_2 [17,18], Al−SiC [19], and Al−AlN [20].

For heat-resistant Al alloys, the evaluating indexes (i.e., the yield strength and elongation at room temperature) are insufficient to link their HT properties. Therefore, the creep performance is required to reflect comprehensive HT performance of materials [21−24]. Typically, the creep controlling mechanism can be revealed by analyzing the steady-state stage of creep. The stress sensitivity coefficient (n) acquired from the slope of steady-state creep rate vs stress curve (Brevity for 'creep curve' hereafter) reflects the creep controlling mechanism [22]. Generally, the creep is controlled by dislocation climb at n=~5 [25,26].

With the diversification of optimizing methods applied on materials, the precipitation-strengthened alloys and particles-reinforced composites show significantly improved creep performances [11,27,28]. For example, LAGNEBORG and BERGMAN [29], HAUSSELT and NIX [30] and MCLEAN [31] proposed the threshold stress mechanism to provide a reasonable explanation for the significant dislocation creep improvement in precipitation-strengthened alloys. They believed that the existence of precipitates weakened the dislocation movement in matrix, and thus caused the threshold stress to reduce creep rate. Besides, NARDONE and STRIFF [32], GONZÁLEZ-DONCEL and SHERBY [33] and PARK and MOHAMED [34] found the improved creep performance in particles-reinforced composites. They explained it by the load transfer effect, in which ceramic particles can effectively share external stress, making actual stress acting on the matrix far less than the applied stress.

In conclusion, the understanding of creep process is not only the analysis on creep curve, but also the establishment of appropriate mathematical model or description according to creep behavior. Therefore, a suitable method is required to describe a general dislocation creep behavior. Generally, the creep behavior and controlling mechanism can be understood using the coupling modification in combination with the threshold stress and load transfer effect [35,36].

Among optimization methods for the heat-resistant Al alloys, the eutectic Al−1.75wt.%Fe−1.25wt.%Ni (Brevity for "Al−Fe−Ni" hereafter) alloy shows excellent thermal stability [37]. In our former work [14], the Al_9FeNi eutectic frame can remain stable for a long time at 400 °C. Nevertheless, the creep performance of this eutectic alloy is rarely studied, and the controlling mechanism is lacking of description to our knowledge. Therefore, this work applies the coupling modification method for analyzing the dislocation creep of the Al−Fe−Ni alloy. In combination with microstructure characterizations and analyses by finite element method (FEM), the creep controlling mechanisms are discussed in depth. Above all, this work reveals the dislocation creep of eutectic Al−Fe−Ni alloy in a more quantitative way. Such analysis on creep behavior is helpful to understanding the controlling creep mechanisms in other eutectic systems.

2 Experimental

2.1 Sample preparation

The sample for the creep test was Al−1.75wt.%Fe−1.25wt.%Ni eutectic alloy. The alloy was prepared by the conventional casting process. The specific preparation process was proposed in Refs. [14,15]. Afterwards, the as-cast sample was machined into dog-bone specimen with 6 mm in diameter and 24 mm in gauge length.

2.2 Creep test

Creep test was performed on an electronic creep testing machine (RDL50) in the air. Before creep test, the sample was held at the set temperature for 0.5 h. To study the creep behavior variation with the change of stress, the steady creep rates at certain stress were the main data obtained by creep test. Therefore, the total creep time was controlled to acquire the steady-state creep rate, and 30 h was sufficient in most cases. To avoid the influence of previous deformation on the creep rate, the single stress condition was applied to acquiring the creep rate.

2.3 Microstructure characterization

The eutectic structures before and after creep were characterized by the scanning electron microscopy (SEM, TESCAN MAIA3) and the transmission electron microscopy (TEM, JEM−2100F). The morphology variations of eutectic phase during creep were presented by SEM images, and the interaction between eutectic phase and

dislocation was presented by TEM characterization.

2.4 Construction of model by finite element method

The FEM analysis was applied to simulating the structure of this eutectic alloy. In Al−Al_9FeNi eutectic structure, the Al_9FeNi phases present the needle-like shape, and they penetrate the whole grain to the length of tens of microns [14,15]. Therefore, the model assumes that the eutectic phase is uniformly distributed in matrix at the direction of cross section. Meanwhile, all the phases in an elementary model are at the same height as the matrix in the longitudinal section. This model can only simulate a single grain, and our as-cast alloy usually has a polycrystalline structure. Although the actual situation is influenced by anisotropy, the model is sufficient to explain the general characteristics of eutectic structure.

The volume fraction of eutectic Al_9FeNi phase in Al−Fe−Ni alloy is 8.4% [15]. Therefore, when the eutectic phase is set as a cylinder with a diameter of 300 nm in cross section, the matrix can be set as a square with side length of 1835 nm. Besides, the model height is set as the twice of the side length. The coefficient of thermal expansion (CTE) for Al matrix is $23.2\times10^{-6}\ °C^{-1}$ at room temperature, and that for AlFeNi alloy is $23\times10^{-6}\ °C^{-1}$ acquired by test. Then, the CTE for Al_9FeNi phase is estimated as $21.3\times10^{-6}\ °C^{-1}$ by rule of mixtures. Through our FEM analyses, it is confirmed that CTE has little effect on the final load distribution behavior between Al and Al_9FeNi phase. Thus, the CTE for each phase at HTs remains unchanged for simplification. The eutectic phase is assumed to experience the elastic deformation all along, but the Al matrix undergoes an elastoplastic deformation. The elastoplastic curves of Al matrix follow the constitutive relationship given in the literature [38]. The Al_9FeNi phase has the elastic modulus of 125 GPa for 300 °C and 113.9 GPa for 400 °C, respectively. These values are extrapolated from the elastic modulus of eutectic phase at different temperatures [39,40]. During the simulation, the sample was heated to 300 or 400 °C, and then uniaxial tensile stress was applied along the longitudinal direction of eutectic phase. The total applied stress was used to control the deformation process, and the stress was controlled as the same at different temperatures.

3 Methods for analyzing creep behavior

The evaluation of creep behavior is mainly based on the analysis of the creep curves experimentally derived. For example, the creep curve of pure metal can be described by the creep constitutive equation, which is provided as [22,23]

$$\dot{\varepsilon} = A\sigma^n \exp[-Q/(RT)] \tag{1}$$

where $\dot{\varepsilon}$ is creep rate at steady-state; A is a constant; σ is the applied stress; n is the stress sensitivity coefficient; Q is the creep activation energy; R is molar gas constant; T is the temperature.

Normally, creep is generally considered to be controlled by different mechanisms depending on the n value [22] at different creep processes. Herein, the dislocation creep process attracts more attention, and n is usually taken as 4.4 for dislocation creep of pure Al [41].

For heat-resistant Al alloy, their creep performances are greatly improved [29−32]. The curve shows a feature that the steady-state creep rate decreases significantly with the reduced stress, making n much higher than 4.4. Correspondingly, the creep theory and creep constitutive equation is developed to describe this transformation [31]:

$$\dot{\varepsilon} = A\sigma^n = B(\sigma - \sigma_{\text{th}})^{4.4} \tag{2}$$

where B is a constant.

Herein, the newly introduced parameter of threshold stress (σ_{th}) is originated from the interaction between dislocations and dispersed particles, reflecting the ability of dispersed particles reinforced alloys to resist creep deformation.

Normally, the specific value of threshold stress is estimated by analytical calculation, rather than direct experimental measurement. The calculation of threshold stress is a refitting process, which involves with the coordinate transformation of creep curves (Fig. 1). In this process, there are several steps required.

(1) The initial strain rates are required to change to $\sqrt[4.4]{\dot{\varepsilon}}$ (The stress sensitivity coefficient of pure Al is 4.4 [41]). Thus, the relationship between strain rate and stress can be rewritten in the $\sigma-\sqrt[4.4]{\dot{\varepsilon}}$ coordinate system.

Specifically, we assume a creep curve of slope n on a lg$x$−lg$y$ coordinate system (Fig. 1(a)). The curve can be described as $\dot{\varepsilon} = A_1\sigma^n$.

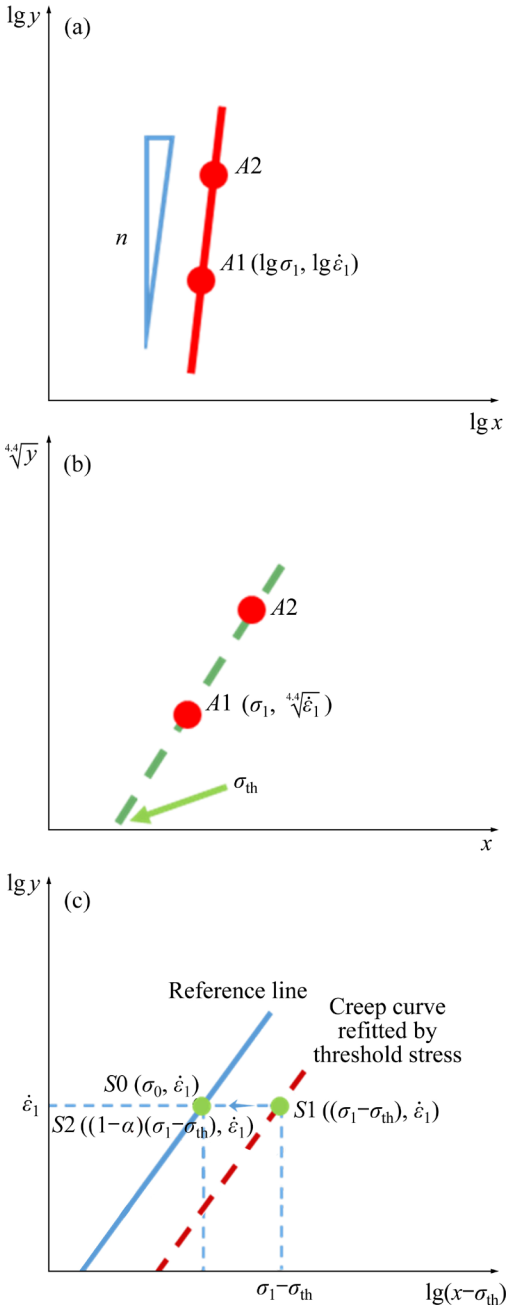

Fig. 1 Creep curve with stress sensitivity coefficient n (a), linear extrapolation method to obtain threshold stress (b) and calculation for load transfer coefficient (c)

In this creep curve, an initial point is assumed as $A1$ ($\lg\sigma_1$, $\lg\dot{\varepsilon}_1$). Then, an increment (δ) is introduced to the stress of $A1$, and thus the Point $A2$ at creep curve can be given as

$$\begin{cases}\lg\sigma_2=\lg\sigma_1+\delta\\ \lg\dot{\varepsilon}_2=n(\lg\sigma_1+\delta)+B\end{cases} \tag{3}$$

Then, both points are transformed to the $x-\sqrt[4.4]{y}$ coordinate system (Fig. 1(b)). Therefore, two points are written as (σ_1, $\sqrt[4.4]{\dot{\varepsilon}_1}$) and ($10^{\delta}\sigma_1$, $\sqrt[4.4]{10^{n\delta}\cdot\dot{\varepsilon}_1}$)

(2) The transformed points are refitted with the straight line: $y=ax+b$.

In the refitting process (Fig. 1(b)), the refitted line ($y=ax+b$) is intersected with x axis to obtain the threshold stress.

(3) The threshold stress is the intercept of x axis.

The threshold stress is marked as σ_{th} in Fig. 1(b), and it can be calculated as

$$\sigma_{th}=\left(1-\frac{4.4}{n}\right)\sigma_1 \tag{4}$$

When the threshold stress is introduced to the creep constitutive equation, creep curve can be described by the transformed equation (Eq. (2)) [31]. Herein, ($\sigma-\sigma_{th}$) is defined as the effective stress. In this case, the $\dot{\varepsilon}=B(\sigma-\sigma_{th})^{4.4}$ can be regarded as the creep rate of Al matrix generated under effective stress. Because the creep process occurs in Al matrix, this process described by the transformed equation should be close to that of Al matrix which is under an actual stress equal to the effective stress. Since the aim of modifying the creep curve and creep constitutive equation is to describe creep behavior effectively, the final modified creep curve should be consistent with the creep curve of Al matrix.

Sometimes, the application of threshold stress cannot fully explain the feature of some creep curves. For example, the creep curve refitted by threshold stress in Fig. 1(c) may not fall on the actual creep curve of Al matrix, which is presented by the reference line. However, these curves should parallel with each other, as they possess the same stress sensitivity coefficient (n=4.4). Thus, their relative positions are adjusted by introducing a coefficient before the term with stress. This coefficient is called as the load transfer coefficient, which is calculated according to the relative position relation between refitted creep curve and creep curve of pure Al (reference line) [32−36]. This integrated method is called as the coupling modification.

Subsequently, the calculation of coupling modification is provided. Firstly, the threshold stress (σ_{th}) can be calculated according to Figs. 1(a, b). In Fig. 1(c), the creep curve refitted by

the subtraction of threshold stress is shown as the dotted red line. Meanwhile, the creep constitutive equation can be written as Eq. (2), and the Point $A1$ should be altered to Point $S1$ ($\sigma_1-\sigma_{th}$, $\dot{\varepsilon}_1$) with n=4.4. Corresponding to Point $S1$, there is the Point $S0$ (σ_0, $\dot{\varepsilon}_1$) on the reference line.

Here, the load transfer coefficient is introduced as

$$\alpha = 1 - \frac{\sigma_0}{\sigma_1 - \sigma_{th}} \tag{5}$$

Hence, the Point $S1$ can be changed to $S2$ $\left[\left(\frac{\sigma_0}{\sigma_1-\sigma_{th}}\right)\cdot(\sigma_1-\sigma_{th}),\ \dot{\varepsilon}_1\right]$, which is $[(1-\alpha)(\sigma_1-\sigma_{th}),\ \dot{\varepsilon}_1]$, and the creep constitutive equation can be modified to

$$\dot{\varepsilon} = A_3[(1-\alpha)(\sigma-\sigma_{th})]^{4.4} = A_3\left\{\left[1-\left(1-\frac{\sigma_0}{\sigma_1-\sigma_{th}}\right)\right](\sigma-\sigma_{th})\right\}^{4.4} \tag{6}$$

4 Results

4.1 Microstructure evolution of Al−Fe−Ni alloy during creep

The microstructure feature of Al−Fe−Ni alloy has been illustrated in literature [14,15]. In detail, the SEM images of eutectic Al−Al_9FeNi structure before (Fig. 2(a)) and after (Fig. 2(b)) creep are both exhibited. Both images are taken from the surface perpendicular to the direction of applied force. Although some holes or damages may appear at local areas (Fig. 2(b)), the overall morphology of crept eutectic structure shows little change. Therefore, the basically unchanged morphology means the creep mainly within the steady-state creep stage.

In the higher magnified micrographs, the needle-like Al_9FeNi phases are parallel to each other in cast alloy (Fig. 2(c)), but show the broken and distorted morphologies after creep (Fig. 2(d)). The broken eutectic phase originates from being

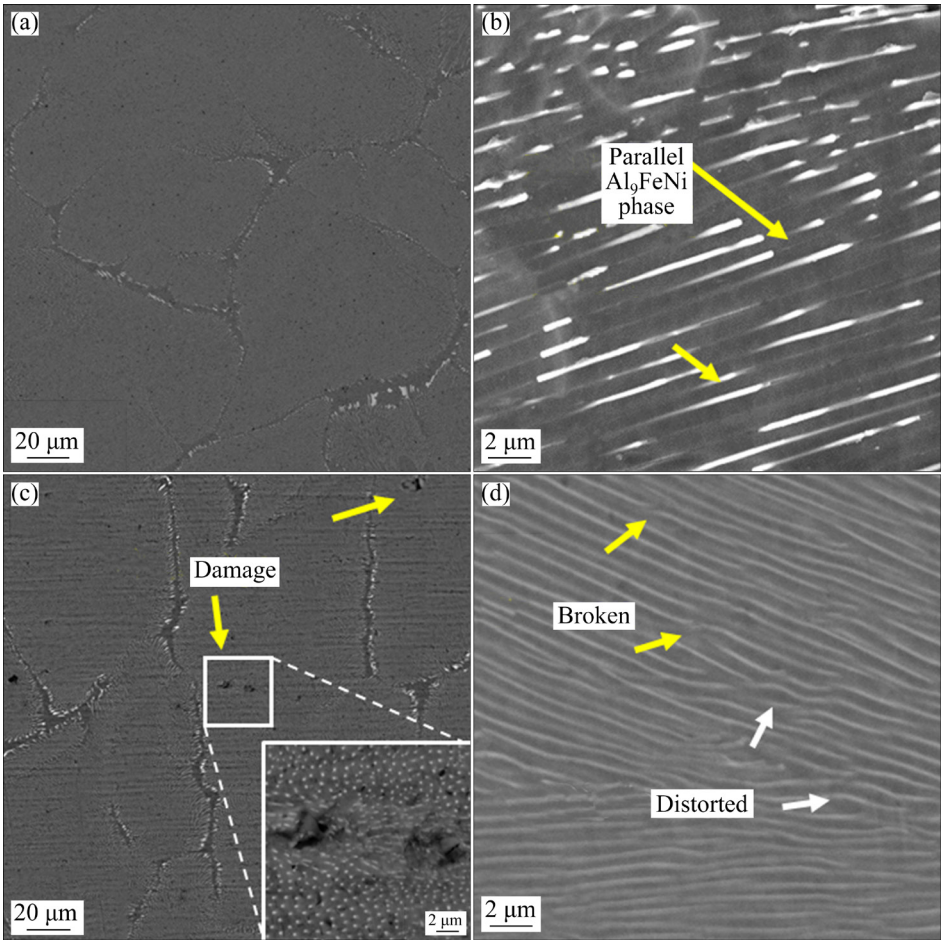

Fig. 2 SEM images of Al−Fe−Ni alloy (a, c) and eutectic phases (b, d) before (a, b) and after (c, d) creep at 30 MPa and 300 °C

subjected to the normal stress, suggesting that the eutectic phase should share the load from Al matrix during creep. The distorted Al_9FeNi phase is caused by the applied shear stress, which may be derived from the interaction between Al_9FeNi phase and dislocation.

The TEM image acquired from the sample after 300 °C creep exhibits the interaction between dislocations and eutectic Al_9FeNi phases. Figure 3(a) shows that the dislocations are entangled around Al_9FeNi phase. This interaction demonstrates that the eutectic phase possesses the ability to impede dislocation movement. Figure 3(b) presents that dislocations shear into the eutectic phase successively and form ordered arrangement, implying that such phase can accommodate dislocation cutting inside to some extent. Figure 3(c) shows the detail of a dislocation shearing into the eutectic phase by the weak-beam dark-field image. Furthermore, the interaction between dislocations and eutectic phases is taken under different imaging conditions to further reveal the dislocation shearing into eutectic phase (Figs. 3(d−f)). Different operation vectors ***g*** confirm the existence of dislocations. The coincidence between dislocations and eutectic phases confirms the possibility of dislocation shearing into eutectic phase. These results indicate the complex interaction between dislocations and eutectic phases.

4.2 Application of coupling modification to analyzing creep behavior of Al−Fe−Ni eutectic alloy at 300 °C

Figure 4(a) presents the creep data of Al−Fe−Ni alloy at 300 °C with the applied stress from 15 to 45 MPa. In detail, the n values are changed with applied stress, reflecting the variation of creep mechanisms. Furthermore, this variation can be divided into three parts.

(1) When the applied stress is beyond ~40 MPa, n changes significantly with the stress. It is often referred to the power law breakdown [22]. During this process, the material undergoes the rapid plastic deformation, and the time effect on the deformation is usually less significant.

(2) When the applied stress is from 25 to 40 MPa, little change of n appears (Fig. 4(a)). In general, the creep here is controlled by dislocation

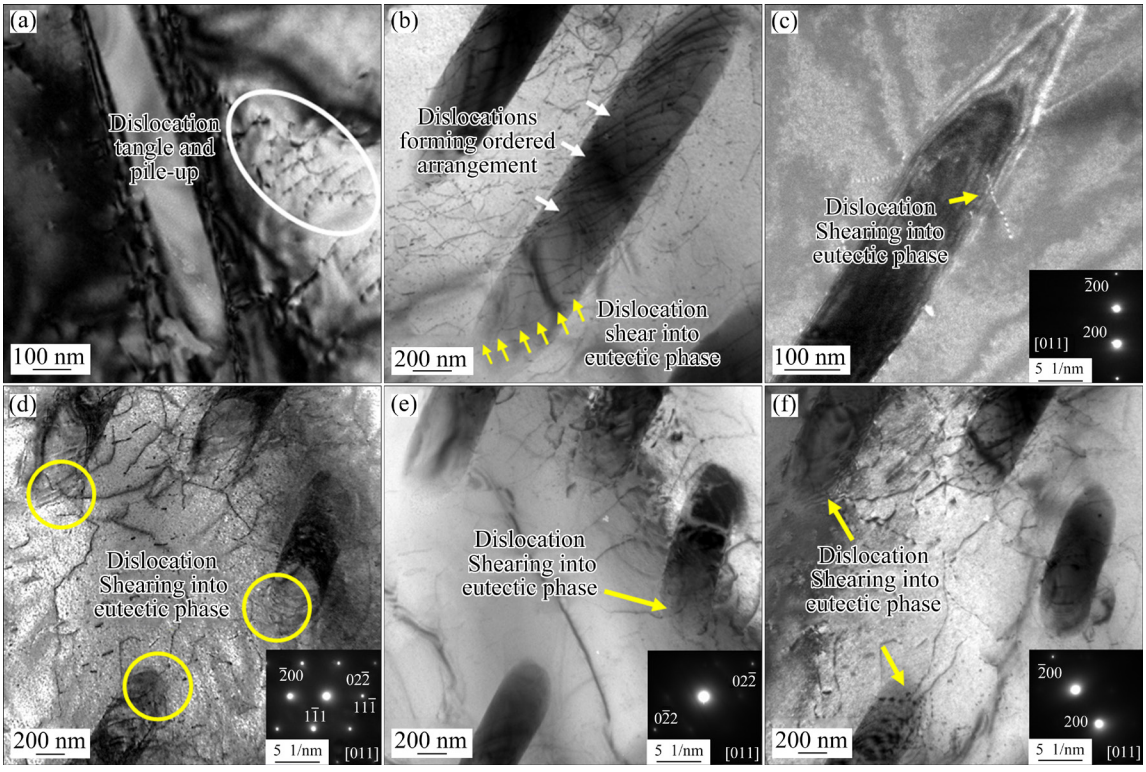

Fig. 3 Interaction between dislocation and eutectic phase: (a) Dislocation tangle and pile-up around eutectic phase; (b) Dislocations shearing into eutectic phase and forming ordered arrangement; (c) Weak-beam dark-field of dislocation shearing into eutectic phase (Interaction of dislocation shearing into eutectic phase under different shooting conditions); (d) Bright field image; (e) $\boldsymbol{g}$=<02$\bar{2}$>; (f) $\boldsymbol{g}$=<200>

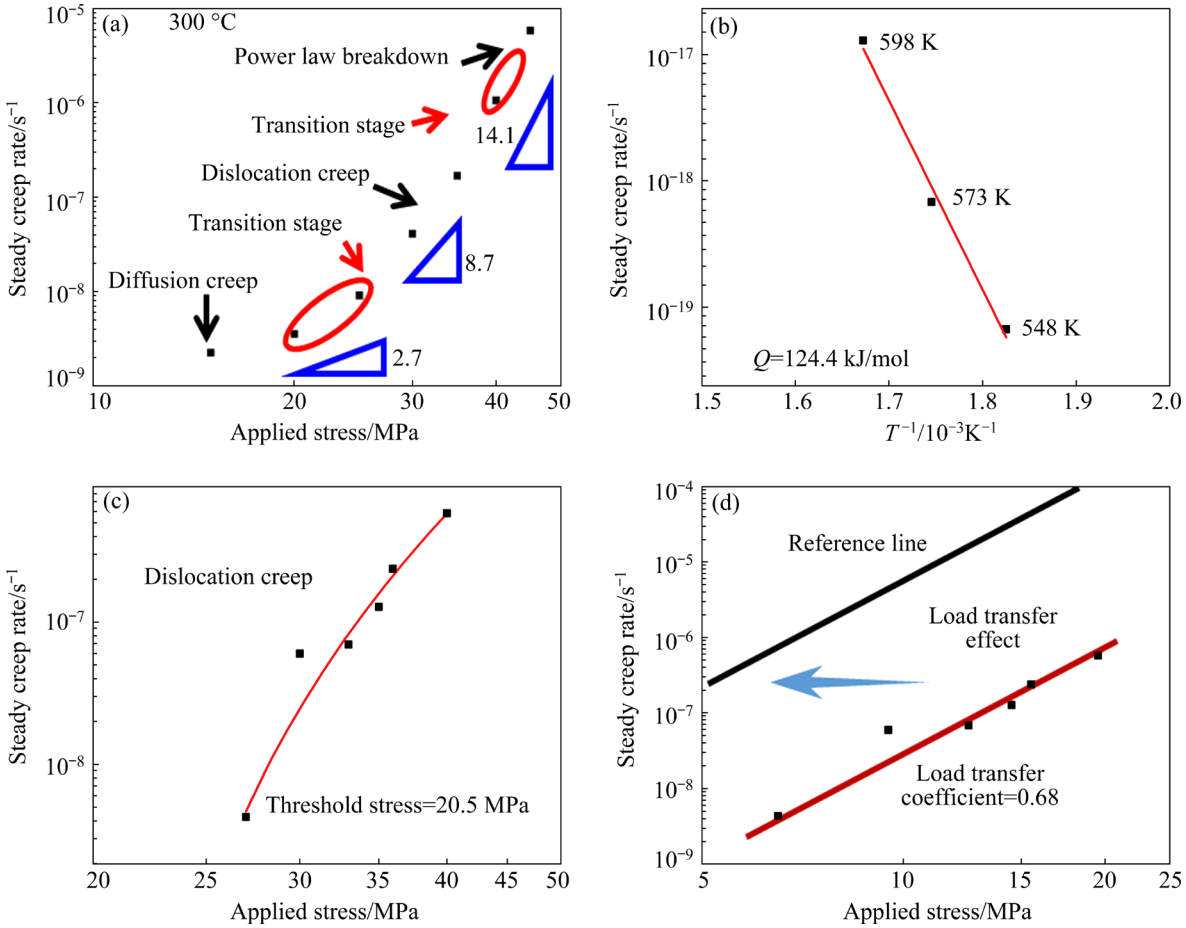

Fig. 4 Creep data of Al−Fe−Ni alloy at 300 °C (a), creep rate vs reciprocal of temperature under 30 MPa at 548−598 K (b), dislocation creep curve of Al−Fe−Ni alloy at applied stress of 27−40 MPa (c), and dislocation creep behavior of Al−Fe−Ni alloy by coupling modification at 300 °C (d)

movement, which is deemed as dislocation creep. For pure Al, n is ~4.4 during this stage [41]. If n is much larger than 4.4, the threshold stress is introduced to explain this phenomenon.

(3) When the applied stress is lower than ~25 MPa, n becomes further smaller. During this stage, the diffusion becomes the controlling mechanism, which is often referred to diffusion creep. Since the change of creep rate with the stress variation is no longer significant, it is in a sense that the creep rate almost reaches the slowest limitation. There is a transition stage between different creep stages, and the transition is accomplished gradually.

Herein, the threshold stress is applied to explaining the abnormal large n (8.7) of dislocation creep (Part II) in Al−Fe−Ni alloy. However, its value cannot be obtained by experiment directly and it must be acquired by calculation at present. Apart from the calculation method itself, the incorporation of data from neighboring stages should also result in calculation inaccuracy of threshold stress. To avoid the influence of different creep stages on the analysis of dislocation creep, the selection of stress range should avoid the transition stage. Namely, the transition stress should be carefully identified to conform to the dislocation creep stage.

Figure 4(b) shows the creep rate versus temperature under a same stress. The temperature interval is 25 °C, and the stress is 30 MPa. The activation energy is calculated as 124.4 kJ/mol at 300 °C, suggesting that the creep is controlled by the self-diffusion based dislocation movement.

Figure 4(c) shows the creep curve of the dislocation creep with the applied stress from 27 to 40 MPa, and the intervals of the applied stress are shortened to further reveal creep behavior. Herein, threshold stress is calculated as ~20.5 MPa, and n is 4.4 for Al referred to literature [41]. Overall, the creep curve of the dislocation creep is refitted

(Fig. 5(d)), and the creep constitutive equation is shown as

$$\dot{\varepsilon} = A_1(\sigma - 20.5)^{4.4} \quad (7)$$

Actually, the refitted creep curve (Fig. 4(d)) cannot meet with the creep curve of Al matrix. Furthermore, a load transfer coefficient (α) is introduced to explain this phenomenon, which is calculated as α=0.68. Thus, the creep constitutive equation can be written as

$$\dot{\varepsilon} = A_2((1-0.68)(\sigma - 20.5))^{4.4} \quad (8)$$

4.3 Application of coupling modification to analyzing creep behavior of Al−Fe−Ni eutectic alloy at 400 °C

Figure 5(a) presents the creep data of Al−Fe−Ni alloy at 400 °C with the applied stress from 5 to 30 MPa. According to the n variation with the changed applied stress, the creep curve can be divided into three parts: (1) The larger applied stress (≥25 MPa) is related to the power law breakdown stage. The increased n suggests that the creep is approaching the power law breakdown stage yet not fully entered; (2) For the smaller applied stress (≤15 MPa), the atom diffusion gradually becomes the controlling mechanism for creep; (3) For the applied stress from 15 to 25 MPa, the dislocation creep (n=7.5) is identified, and more test results are given in Fig. 5(c).

Similarly, Fig. 5(b) shows the creep rate versus temperature under a same stress. The stress condition is 20 MPa for 400 °C, and the temperature interval is 25 °C. The activation energy is calculated as 374.8 kJ/mol. Though the activation energy at 400 °C is much higher, the creep is still considered to be controlled by the self-diffusion based dislocation movement. This phenomenon is very common in particles reinforced composites, in which the mechanism like load transfer plays the main role in strengthening the matrix [32−34].

According to the provided creep curve (Fig. 5(c)), the threshold stress is calculated as 12.6 MPa for dislocation creep. Therefore, the creep

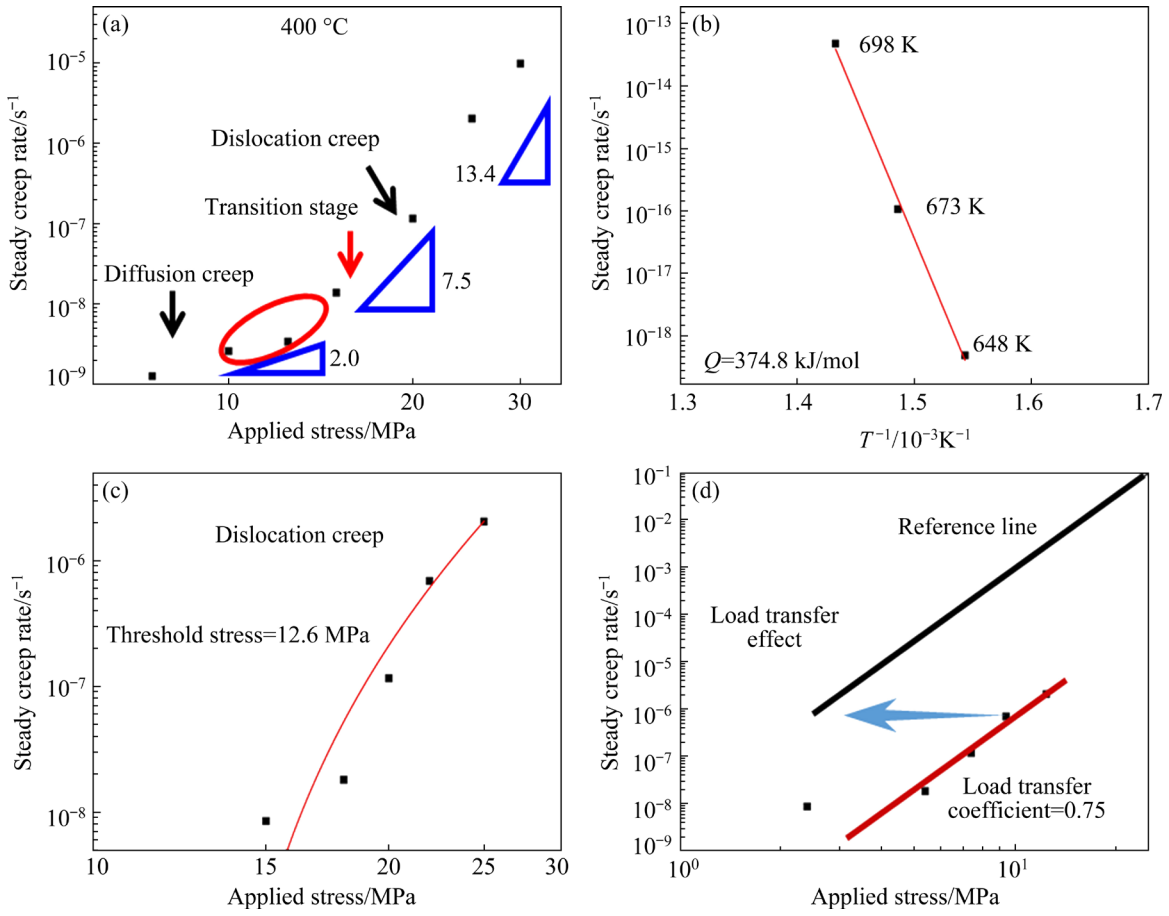

Fig. 5 Creep data of eutectic Al−Fe−Ni at 400 °C (a), creep rate vs reciprocal of temperature under 20 MPa at 648−698 K (b), dislocation creep curve of Al−Fe−Ni at applied stress of 15−25 MPa (c), and dislocation creep behavior of eutectic alloy by coupling modification at 400 °C (d)

constitutive equation can be provided as

$$\dot{\varepsilon} = A_3(\sigma - 12.6)^{4.4} \quad (9)$$

The threshold stress of Al−Fe−Ni alloy at 400 °C is lower than that at 300 °C. This is an accepted situation that threshold stress decreases with the increasing temperature, which is caused by the reduced shear modulus at HTs [22,42].

Subsequently, the refitted creep curve is obtained after the introduction of threshold stress (Fig. 5(d)). This refitted creep curve still cannot meet with the creep curve of Al matrix. Therefore, the load transfer coefficient (α) is calculated as 0.75, and the creep constitutive equation is written as

$$\dot{\varepsilon} = A_4((1 - 0.75)(\sigma - 12.6))^{4.4} \quad (10)$$

Herein, the load transfer coefficient (α) at 400 °C is a bit larger than that at 300 °C, suggesting that the load transfer effect should be accounted more at HTs.

5 Discussion

5.1 Origin of threshold stress and load transfer effect in eutectic alloy

From the mathematical analysis of the creep curve, the coupling modification is necessary for an adequate description of a general creep behavior. Either the introduction of threshold stress or the load transfer effect is intended to describe a particular kind of creep behavior. In some complex strengthening alloy or composite systems, the creep behavior should be understood in a comprehensive way.

Specifically, the necessity of the coupling modification for analyzing the creep behavior of eutectic alloy is affirmed, according to the creep curves and related analyzing process. However, the coupling modification only explains the effect of multiple mechanisms on creep behavior. It does not explain the origin of the improved creep behavior.

Since the eutectic phase is the only strengthening phase in the eutectic alloy, it should have multiple roles to enhance creep resistance of matrix. Furthermore, the microstructure evolution after creep can be referenced for investigating the origin of controlling creep mechanisms (Figs. 2−3). These results indicate the complex interaction between dislocations and eutectic phases. Therefore, the improvement induced by eutectic phase on creep is investigated from both threshold stress mechanism and load transfer mechanism.

5.1.1 Origin of threshold stress from eutectic phase in eutectic alloy

Normally, the threshold stress provided by reinforcing phases can be divided into several types.

(1) The threshold stress originates from the change in the state of the dislocation itself. These additional stresses are caused by the enhancement in the length of dislocation line, when the dislocation climbs over the precipitate [29,31]. According to the length increment of dislocation line, the interaction mechanisms between dislocations and precipitates are divided into local climb and global climb.

(2) The second type of threshold stress derives from either energy or strain fields acting on the dislocation produced by the particle. The effect of energy field on the dislocation movement can be traced back to the detachment mechanism proposed in creep process of incoherent phase strengthened alloys [43,44]. Since the energy of incoherent phase interface is lower than that of matrix, dislocations can easily reach the interface and travel along the interface to the departure direction. However, there is more energy required to overcome the increasing energy field when the dislocation leaves the interface. Thus, the threshold stress is caused by the energy barrier.

Furthermore, the effect of strain field on the dislocation movement can be recognized from the creep process of the coherent phase strengthened alloys [45]. The threshold stress results from the interaction between the dislocation and coherent interface. However, there are inevitable lattice mismatches and distortions at the interface, due to the existing difference from lattice constants between matrix and coherent phase. Therefore, a coherency strain field can be generated nearby the interface [46]. This strain field should exert extra stress on the surrounding dislocation, and thereby induce threshold stress.

(3) The threshold stress can also stem from the particles that can be shared by the dislocation. The shear modulus of the particle is usually larger than the matrix, and the larger stress is required when the dislocation shears into the particle. Hence, the threshold stress is produced. In addition, the energy required to form the new interface or antiphase

boundary after the particles sheared by dislocation can also be the source of threshold stress. In the available reports, the particle shear is an important strengthening mechanism for reinforcing the metal matrix at room temperature [46]. Therefore, this mechanism should also be used as the cause for threshold stress to reveal the improvement of creep properties.

For the Al_9FeNi eutectic phase in Al−Fe−Ni alloy, it has a needle-like morphology. Its diameter on the cross section is ~300 nm and the length on the longitudinal direction is tens of microns [14]. Normally, it is quite difficult for dislocation to climb over the eutectic phase. However, it still happens at the edge of eutectic phase. Due to the nano-scale for cross section, it is possible for the interface to impede the dislocation movement by dislocation climb mechanism or detachment mechanism. Nevertheless, this may be the origin of threshold stress, and it may contribute only a little to the total threshold stress.

On the other hand, the TEM image (Figs. 3(b−f)) demonstrates that the dislocation shears into the eutectic phase when the dislocation interacts with these phases. With the dislocation further shearing into the phase and piling up along the interface, the eutectic phase finally becomes broken and distorted (Fig. 2(d)). Because the Al_9FeNi phase has the micron-scale in the longitudinal section, there is a high probability for dislocation to cut into the phase. In general, the third type of threshold stress may also be one of the origins of threshold stress in eutectic alloys.

5.1.2 Origin of load transfer effect from eutectic phase in eutectic alloy

According to the coupling modification, the load transfer effect can be produced by eutectic phase in eutectic alloys apart from the threshold stress. Unlike the threshold stress relies on the dislocation movement, the load transfer effect works as soon as the stress is applied on the materials. Normally, the eutectic alloy has a large volume fraction of eutectic phase, which can be regarded as the composite material. In this composite, the strengthening mechanism strongly depends on the morphology of reinforcing phase, because the morphological feature can influence the competition between Orowan strengthening mechanism and the load transfer effect of the reinforcing phase. When the aspect ratio of the reinforcing phase is relatively large (This accords to the morphological feature of Al_9FeNi phase), the load transfer plays a vital role in strengthening the matrix [47].

In this work, a brief analysis is made from the view of coordinated deformation to explain the origin of load transfer effect. Based on the eutectic structure and physical properties of each phase, the model of the Al−Al_9FeNi eutectic structure is established by FEM, and relevant parameters of the model are provided before. The stress distribution among the eutectic structure under a stress of 32 MPa at 300 °C is shown in Fig. 6(a), and the stress on eutectic phase is much greater than that on Al matrix.

When the stress applies on the eutectic structure, such structure shows elastic deformation firstly. Influenced by coordinated deformation, the deformation of the eutectic Al_9FeNi phase is the same as the eutectic Al matrix. Thus, per unit volume eutectic Al_9FeNi phase should be subjected to greater stress due to its larger elastic modulus [39].

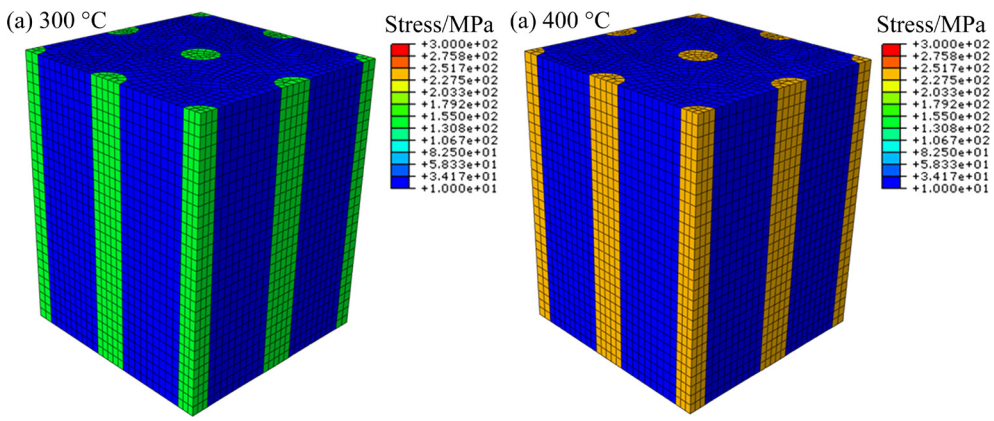

Fig. 6 Finite element model of Al−Al_9FeNi structure with corresponding stress distribution for this structure under 32 MPa at 300 °C (a) and 400 °C (b)

The stress on each phase multiplied by the volume fraction of each part is the total stress applied on the eutectic structure. Therefore, the actual stress acting on the low modulus part (eutectic Al matrix) should be lower than the applied stress on eutectic structure. It appears that the high modulus part (eutectic Al_9FeNi phase) shares the stress acting on the matrix. The stress distribution in eutectic structure is deemed as the load transfer effect, and the eutectic Al_9FeNi phase plays an effective role in sharing the load of eutectic Al matrix. Within the creep process, the load transfer effect of eutectic phase still exists despite eutectic Al matrix undergoes plastic deformation.

Since the eutectic phase has nano-scale cross section and micron-scale longitudinal section at the same time, these phases can not only effectively impede the dislocation movement and cause the threshold stress effect, but also cause the load transfer effect. This discussion reveals the origin of threshold stress and load transfer effect from the view of physical nature, and reveals the necessity of coupling modification to describe the creep behavior of eutectic alloy.

5.2 Effects of temperature on threshold stress and load transfer effect in eutectic alloy

Overall, the intensified atomic vibration caused by temperature enhancement should inevitably lead to the reduced shear modulus of materials [41]. Due to the differences in either crystalline structures or atomic properties, the temperature effect on shear modulus should be different between the reinforcing phase and matrix. Therefore, the temperature effects on threshold stress and load transfer effect are different.

For the threshold stress arising from the dislocation itself or the related energy or strain field variations, the corresponding temperature influence is usually consistent with the related effect on shear modulus of the matrix. The dislocation movement becomes easier with the reduced shear modulus of the Al matrix, thus the threshold stress should inevitably decrease. Furthermore, the threshold stress derived from particles sheared by the dislocation is also affected by the reinforcing phase, and its variation may be more significant than the change of the matrix shear modulus.

In the Al−Fe−Ni eutectic alloy (Fig. 4(c) at 300 °C) and 5(c) (at 400 °C)), the threshold stress is decreased with the increasing temperature. The reduced shear modulus of Al matrix with elevated temperatures may be the first reason [42]. Besides, the decreased shear modulus of the reinforcing phase is the second reason for the reduced threshold stress. Experimentally, the eutectic Al_9FeNi sheared by the dislocation is observed in this eutectic alloy. Therefore, the decreased shear modulus of eutectic phase may also be the reason for reduced threshold stress. However, the specific explanation for the evolution of threshold stress with temperature needs further experiments to be studied separately.

For the load transfer effect, the elastic modulus between the reinforcing phase and matrix is the main origin. Due to the linear relationship between elastic modulus and shear modulus in metals, the load transfer effect is obviously affected by the difference in shear modulus between the reinforcing phase and matrix. As the temperature increases, the shear modulus of the reinforcing phase (i.e., ceramics or intermetallics) with higher melting point should have a smaller reduced tendency than the metal matrix with lower melting point [40]. The differentiated decreased tendencies on both phases can decide the temperature effect on load transfer effect.

Experimentally, the load transfer coefficient increases with elevated temperature (Figs. 4(d) and 5(d)). Theoretically, Fig. 6(b) shows the model of eutectic Al−Al_9FeNi structure under a stress of 32 MPa at 400 °C. The Al_9FeNi phase at 400 °C is subjected to greater stress compared to that at 300 °C. This indicates a stronger load transfer effect at 400 °C, which shows a similar tendency with experimental results. Although the shear modulus of either Al_9FeNi phase or α(Al) matrix decreases with elevated temperature, the diminished shear modulus of Al_9FeNi phase is less severe than α(Al) matrix [40]. Comparatively, the Al_9FeNi phase can share more stress at HTs, and the load transfer coefficient becomes larger at HTs. To a large extent, the load transfer effect should be a more reliable strengthening mechanism at HTs.

6 Conclusions

(1) The coupling modification demonstrates that dislocation creeps of Al−Fe−Ni eutectic alloy at 300 or 400 °C are both controlled by threshold stress and load transfer effect. The improved creep

performance of eutectic alloy can be explained from different aspects by threshold stress mechanism or load transfer mechanism.

(2) Microstructure characteristics show that threshold stress should originate from the interaction between Al_9FeNi phase and dislocations, and the eutectic phase sheared by the dislocation may be the main reason. However, the threshold stress decreases with the increasing temperature, and the dislocation movement becomes more difficult to be impeded by eutectic phase. The reduced shear modulus of matrix and eutectic phase is the main reason for the decrease of threshold stress.

(3) The Al_9FeNi phase can also play an effective role in transferring load, due to its larger volume fraction and higher modulus. Since the diminished shear modulus of Al_9FeNi phase is less severe than that of Al matrix, the load transfer coefficient becomes larger at HTs. This ensures the eutectic phase to effectively improve the creep resistance of matrix even at HTs.

Acknowledgments

Dr. Ze-yu BIAN wishes to acknowledge the scholarship support from the Chinese Scholarship Council. The authors should appreciate Dr. Li-ming FU for his great help in the creep experiments.

The authors are grateful for the financial supports from the National Natural Science Foundation of China (No. 52071207), the China Postdoctoral Science Foundation (Nos. 2019TQ0193, 2019M661497), the National Key Research and Development Program of China (No. 2018YFB1106302), and Anhui Provincial Engineering Research Center of Aluminum Matrix Composites, China (No. 2017WAMC002).

References

[1] WILLIAMS J C, Jr STARKE E A. Progress in structural materials for aerospace systems [J]. Acta Materialia, 2003, 51: 5775−5799.

[2] KNIPLING K E, DUNAND D C, SEIDMAN D N. Criteria for developing castable, creep-resistant aluminum-based alloys—A review [J]. Zeitschrift Für Metallkunde, 2006, 97: 246−265.

[3] DURSUN T, SOUTIS C. Recent developments in advanced aircraft aluminium alloys [J]. Materials & Design, 2014, 56: 862−871.

[4] SUN Wen-wen, ZHU Yu-man, MARCEAU R, WANG Ling-yu, ZHANG Qi, GAO Xiang, HUTCHINSON C. Precipitation strengthening of aluminum alloys by room-temperature cyclic plasticity [J]. Science, 2019, 363: 972−975.

[5] TIWARY C S, PANDEY P, SARKAR S, DAS R, SAMAL S, BISWAS K, CHATTOPADHYAY K. Five decades of research on the development of eutectic as engineering materials [J]. Progress in Materials Science, 2022, 123: 100793.

[6] ZHANG Jia-ying, FENG Jian, ZUO Li-jie, YE Bing, KONG Xiang-yang, JIANG Hai-yan, DING Wen-jiang. Effect of Sc microalloying addition on microstructure and mechanical properties of as-cast Al−12Si alloy [J]. Materials Science and Engineering A, 2019, 766: 138343.

[7] CHEN B A, LIU G, WANG R H, ZHANG J Y, JIANG L, SONG J J, SUN J. Effect of interfacial solute segregation on ductile fracture of Al−Cu−Sc alloys [J]. Acta Materialia, 2013, 61: 1676−1690.

[8] ZHANG Dong-lan, WANG Jiong, KONG Yi, ZOU You, DU Yong. First-principles investigation on stability and electronic structure of Sc-doped θ'/Al interface in Al−Cu alloys [J]. Transactions of Nonferrous Metals Society of China, 2021, 31: 3342−3355.

[9] SUN Teng-teng, GENG Ji-wei, BIAN Ze-yu, WU Yi, WANG Ming-liang, CHEN Dong, MA Nai-heng, WANG Hao-wei. Enhanced thermal stability and mechanical properties of high-temperature resistant Al−Cu alloy with Zr and Mn micro-alloying [J]. Transactions of Nonferrous Metals Society of China, 2022, 32: 64−78.

[10] SEIDMAN D N, MARQUIS E A, DUNAND D C. Precipitation strengthening at ambient and elevated temperatures of heat-treatable Al(Sc) alloys [J]. Acta Materialia, 2002, 50: 4021−4035.

[11] FULLER C B, SEIDMAN D N, DUNAND D C. Mechanical properties of Al(Sc,Zr) alloys at ambient and elevated temperatures [J]. Acta Materialia, 2003, 51: 4803−4814.

[12] LI Zhen, ZHANG Zhan, CHEN X-Grant. Effect of magnesium on dispersoid strengthening of Al−Mn−Mg−Si (3xxx) alloys [J]. Transactions of Nonferrous Metals Society of China, 2016, 26: 2793−2799.

[13] SUWANPREECHA C, TOININ J P, MICHI R A, PANDEE P, DUNAND D C, LIMMANEEVICHITR C. Strengthening mechanisms in Al−Ni−Sc alloys containing Al_3Ni microfibers and Al_3Sc nanoprecipitates [J]. Acta Materialia, 2019, 164: 334−346

[14] BIAN Ze-yu, DAI Shi-han, WU Liang, CHEN Zhe, WANG Ming-liang, CHEN Dong, WANG Hao-wei. Thermal stability of Al−Fe−Ni alloy at high temperatures [J]. Journal of Materials Research and Technology, 2019, 8: 2538−2548.

[15] BIAN Ze-yu, LIU Ying-tao, DAI Shi-han, CHEN Zhe, WANG Ming-liang, CHEN Dong, WANG Hao-wei. Regulating microstructures and mechanical properties of Al−Fe−Ni alloys [J]. Progress in Natural Science: Materials International, 2020, 30: 54−62.

[16] AKOPYAN T K, BELOV N A, NAUMOVA E A, LETYAGIN N V, SVIRIDOVA T A. Al-matrix composite based on Al−Ca−Ni−La system additionally reinforced by L12 type nanoparticles [J]. Transactions of Nonferrous Metals Society of China, 2020, 30: 850−862.

[17] HUANG Min-hwa, LI Xian-feng, YI Hong-zhan, MA Nai-heng, WANG Hao-wei. Effect of in situ TiB_2 particle reinforcement on the creep resistance of hypoeutectic Al−12Si alloy [J]. Journal of Alloys and Compounds, 2005, 389: 275−280.

[18] DAI Shi-han, BIAN Ze-yu, WANG Ming-liang, WU Yi, CHEN Dong, LI Hong-ping, WANG Hao-wei. The high-temperature creep behavior of in-situ TiB_2 particulate reinforced $Al_{12}Si_4Cu_2NiMg$ composite [J]. Metals, 2018, 8: 917.

[19] HONG Yu, WANG Wu-jie, LIU Jia-qin, TANG Wen-ming, WU Yu-cheng. Effect of porosity and interface structures on thermal and mechanical properties of SiC_p/6061Al composites with high volume fraction of SiC [J]. Transactions of Nonferrous Metals Society of China, 2019, 29: 941−949.

[20] MA Xia, ZHAO Yong-feng, ZHAO Xiao-jun, NIE Jin-feng, CHEN Hou-wen, LIU Xiang-fa. Mechanisms on the outstanding high temperature plasticity of AlN_p/Al−0.4Cu composites induced by cryogenic treatment [J]. Journal of Alloys and Compounds, 2019, 770: 755−764.

[21] ZHANG Jia-ying, ZUO Li-jie, FENG Jian, YE Bing, KONG Xiang-yang, JIANG Hai-yan, DING Wen-jiang. Effect of thermal exposure on microstructure and mechanical properties of Al−Si−Cu−Ni−Mg alloy produced by different casting technologies [J]. Transactions of Nonferrous Metals Society of China, 2020, 30: 1717−1730.

[22] KASSNER M E. Greep fracture [M]//Fundamentals of Creep in Metals and Alloys [M]. 2nd ed. Amsterdam: Elsevier, 2008: 221−246.

[23] BETTEN J. Creep mechanics [M]. 3rd ed. Berlin: Springer, 2008.

[24] TANG Jian-guo, YU Bo, ZHANG Jin, XU Fu-shun, BAO Chong-jun. Effects of pre-deformation mode and strain on creep aging bend-forming process of Al−Cu−Li alloy [J]. Transactions of Nonferrous Metals Society of China, 2020, 30: 1227−1237.

[25] WEERTMAN J R. Theory of steady-state creep based on dislocation climb [J]. Journal of Applied Physics, 1955, 26: 1213−1217.

[26] KASSNER M E, PÉREZ-PRADO M T. Five-power-law creep in single phase metals and alloys [J]. Progress in Materials Science, 2000, 45: 1−102.

[27] GRIFFITHS S, CROTEAU J R, ROSSELL M D, ERNI R, LUCA A D, VO N Q, DUNAND D C, LEINENBACH C. Coarsening and creep resistance of precipitation-strengthened Al−Mg−Zr alloys processed by selective laser melting [J]. Acta Materialia, 2020, 188: 192−202.

[28] LI He, ZHAN Li-hua, HUANG Ming-hui, ZHAO Xing, ZHOU Chang, HU Li-bin, HU Zheng-gen, LIU De-bo. A unified constitutive model for multiphase precipitation and multi-stage creep ageing behavior of Al−Li−S4 alloy [J]. Transactions of Nonferrous Metals Society of China, 2021, 31: 1217−1234.

[29] LAGNEBORG R, BERGMAN B. The stress/creep rate behaviour of precipitation-hardened alloys [J]. Metal Science, 1976, 10: 20−28.

[30] HAUSSELT J H, NIX W D. A model for high temperature deformation of dispersion strengthened metals based on substructural observations in Ni−20Cr−2ThO_2 [J]. Acta Metallurgica, 1977, 25: 1491−1502.

[31] MCLEAN M. On the threshold stress for dislocation creep in particle strengthened alloys [J]. Acta Metallurgica, 1985, 33: 545−556.

[32] NARDONE V C, STRIFE J R. Analysis of the creep behavior of silicon carbide whisker reinforced 2124 Al(T4) [J]. Metallurgical Transactions A, 1987, 18: 109−114.

[33] GONZÁLEZ-DONCEL G, SHERBY O D. High temperature creep behavior of metal matrix aluminum-SiC composites [J]. Acta Metallurgica et Materialia, 1993, 41: 2797−2805.

[34] PARK K T, MOHAMED F A. Creep strengthening in a discontinuous SiC−Al composite [J]. Metallurgical & Materials Transactions A, 1995, 26: 3119−3129.

[35] PENG L M, ZHU S J. Creep of metal matrix composites reinforced by combining nano-sized dispersoids with micro-sized ceramic particulates or whiskers [J]. International Journal of Materials and Product Technology, 2003, 18: 215−254.

[36] FERNÁNDEZ R, GONZÁLEZ-DONCEL G. Threshold stress and load partitioning during creep of metal matrix composites [J]. Acta Materialia, 2008, 56: 2549−2562.

[37] PREMKUMAR M K, LAWLEY A, KOCZAK M J. Processing and microstructure of powder metallurgy Al−Fe−Ni alloys [J]. Metallurgical Transactions A, 1992, 23: 3219−3230.

[38] BROWN S B, KIM K H, ANAND L. An internal variable constitutive model for hot working of metals [J]. International Journal of Plasticity, 1989, 5: 95−130.

[39] CHEN C L, RICHTER A, THOMSON R C. Mechanical properties of intermetallic phases in multi-component Al−Si alloys using nanoindentation [J]. Intermetallics, 2009, 17: 634−641.

[40] CHEN C L, RICHTER A, THOMSON R C. Investigation of mechanical properties of intermetallic phases in multi-component Al−Si alloys using hot-stage nanoindentation [J]. Intermetallics, 2010, 18: 499−508.

[41] FROST H J, ASHBY M F. Deformation-mechanism maps: The plasticity and creep of metals and ceramics [M]. 1st ed. Oxford: Pergamon Press, 1982.

[42] CADEK J, KUCHAROVA K, ZHU S J. Threshold stress and load transfer effects in creep of an Al−8.5Fe−1.3V−1.7Si alloy reinforced with silicon carbide particulates-an Al−8.5Fe−1.3V−1.7Si−15SiC_p composite [J]. International Journal of Materials and Product Technology, 2003, 18: 178−198.

[43] ARZT E, WILKINSON D S. Threshold stresses for dislocation climb over hard particles: The effect of an attractive interaction [J]. Acta Metallurgica, 1986, 34: 1893−1898.

[44] RÖSLER J, ARZT E. A new model-based creep equation for dispersion strengthened materials [J]. Acta Metallurgica et Materialia, 1990, 38: 671−683.

[45] KRUG M E, DUNAND D C. Modeling the creep threshold stress due to climb of a dislocation in the stress field of a misfitting precipitate [J]. Acta Materialia, 2011, 59: 5125−5134.

[46] GLADMAN T. Precipitation hardening in metals [J]. Materials Science and Technology, 1999, 15: 30−36.

[47] CHEN B, SHEN J, YE X, JIA L, LI S, UMEDA J, TAKAHASHI M, KONDOH K. Length effect of carbon nanotubes on the strengthening mechanisms in metal matrix composites [J]. Acta Materialia, 2017, 140: 317−325.

耦合修正分析 Al−Fe−Ni 合金蠕变机理

卞泽宇[1,2,3]，朱爱林[1,2]，肖亚开[1,2]，李宇罡[1]，马乃恒[1,4]，卞汉兵[3]，汪明亮[1]，陈 哲[2]，王浩伟[1,2]

1. 上海交通大学 金属基复合材料国家重点实验室，上海 200240；
2. 上海交通大学 材料科学与工程学院，上海 200240；
3. Laboratoire de Génie Civil et Géo-Environnement, Université de Lille, F-59000 Lille, France;
4. 安徽省铝基复合材料工程研究中心，淮北 235000

摘 要：在引入阈值应力和载荷传递系数后，对 Al−Fe−Ni 合金的蠕变本构方程进行耦合修正，描述该合金在 300 和 400 °C 下的位错蠕变。量化结果分析及显微组织表征表明，蠕变过程中位错与共晶相间复杂交互作用是阈值应力的起源。同时，共晶相与基体之间模量的差异引起共晶相分担应力作用。此外，温度对基体及共晶相模量产生的影响差异导致高温时合金阈值应力降低，而应力转移系数增大。这些现象通过有限元模型分析得到进一步的论证。总体而言，共晶合金位错蠕变的控制机理得到了更深层次的量化认识。

关键词：位错蠕变；铝合金；共晶相；应力转移效果；阈值应力

(Edited by Xiang-qun LI)